**1.4 ON THE EFFECTS OF HELIUM-DPA INTERACTIONS ON CAVITY EVOLUTION IN TEMPERED MARTENSITIC STEELS UNDER DUAL ION-BEAM IRRADIATION ——** Takuya Yamamoto, Yuan Wu, G. Robert Odette (University of California Santa Barbara), Kiyohiro Yabuuchi, Sosuke Kondo, Akihiko Kimura (Kyoto University)

## OBJECTIVE

The objective of this research is to characterize how cavities and other microstructural features evolve in irradiated 9Cr tempered martensitic steels (TMS) and nanostructured ferritic alloys (NFA) are affected by the starting microstructure and irradiation variables, including temperature, displacements per atom (dpa), dpa rate and the helium/dpa (He/dpa) ratio.

## SUMMARY

Cavity evolution in normalized and tempered 8Cr martensitic steels (TMS) F82H under $Fe^{3+}$ and $He^{+}$ dual ion beam irradiation (DII) at 500°C was characterized for a number of new dpa and He conditions. The cavity evolution TMS alloy database at 500°C now includes 280 material-dpa-He-dpa rate DII conditions. In summary, key observations on swelling include: a) the $f_v$-dpa trend is controlled by the He/dpa; b) better accounting for local microstructure effects and run-to-run variations partly rationalized the observed large data $f_v$ "scatter"; c) $f_v$ is somewhat lower in the reference case and similar runs; d) $f_v$ is lower in the Ta modified variant of F82H than in the IEA heat and $f_v$ in the latter decreases with increasing cold work.

## BACKGROUND

As reported previously [1-5], we have been carrying out systematic DII studies at 500°C in DuET facility in Kyoto University at various nominal He/dpa and dpa rates (defined at the depth of 600 nm) in TMS and NFA. Here we update the DII database and report an analyses cavity evolution (and swelling) trends in F82H Mod.3 (M3) and IEA TMS encompassing a very wide range of DII dpa, He and He/dpa. We also compared the behavior of F82H to that in the NFA.

## PROGRESS AND STATUS

### Experiment

While details of alloys and DII experiments can be found in [3], Table 1 summarizes nominal He and dpa conditions at two reference depth locations encompassed by the current database. The irradiations targeted two nominal doses, three He/dpa and two dpa rate conditions. Taking advantage of the varying spatial distributions of dpa, He and He/dpa with the example shown Figure 1a, we characterized the microstructures over a very wide range of He and dpa conditions. Figure 1b shows all the available conditions for F82H IEA in both as-tempered and two cold worked conditions and Ta-modified F82H Mod.3 for a wide range of dpa and He/dpa ratios. Here we report TEM quantitative characterization of cavity (bubbles and voids) structures in a series of 100nm slices from near the beginning to beyond the end of the range of the 6.4 MeV $Fe^{3+}$ ions. The specific conditions shown in Figure 1b represent the average dpa, He and He/dpa in each of the 100 nm slices. The dpa are based on SRIM using the Kinchin-Pease with Fe displacement energy of 40 eV [6,7].

## RESULTS

### Void swelling as a function of He and He/dpa and root causes of observed scatter

Here cavity evolution trends as a function of dpa and He/dpa are quantified in terms of average diameter, $\langle d \rangle$, number density, N, and volume fraction, f. Earlier analyses showed that variations in the void $\langle d_v \rangle$ and $N_v$ are less sensitive to local microstructure variations; and that the total $f \approx f_v$. We separate voids from bubbles by assuming a (≈ critical) threshold diameter of 4 nm for the latter. This threshold is not fixed or rigorous, but corresponds to a dip that is often observed between two bubble-void peaks in the cavity size distribution. We have also previously noted that there is significant scatter in the data trends,

including f, which is likely due to variations in the local microstructure and the uncertainty in the irradiation temperature [1].

**Table 1.** Irradiation conditions analyzed in this report.

| Exp ID | Alloys | T ($^{o}$C) | Nominal Condition (@550-650nm) | | | | Peak He (@1000-1100nm) | | |
|---|---|---|---|---|---|---|---|---|---|
| | | | dpa | He (appm) | He/dpa | dpa/s | dpa | He (appm) | He/dpa |
| DI10B1 | FM3 | 500 | 26 | 1210 | 47 | $5.0 \times 10^{-4}$ | 45 | 2100 | 47 |
| DI10B2 | | | 9.9 | 457 | 46 | $5.2 \times 10^{-4}$ | 17 | 795 | 46 |
| DI10B3 | | | 10 | 480 | 47 | $5.1 \times 10^{-4}$ | 18 | 840 | 47 |
| DI13A1 | FM3 | 500 | 26 | 390 | 15 | $5.1 \times 10^{-4}$ | 44 | 670 | 15 |
| DI13B1 | FM3, FIA | 500 | 30 | 848 | 29 | $1.5 \times 10^{-3}$ | 51 | 1467 | 29 |
| DI13B2 | FIB, FID | 500 | 27 | 730 | 28 | $1.5 \times 10^{-3}$ | 46 | 1262 | 28 |
| DI14A1 | FM3, FIA | 500 | 30 | 1340 | 45 | $1.3 \times 10^{-3}$ | 52 | 2320 | 45 |
| DI14A2 | FIB, FID | 500 | 30 | 1400 | 46 | $1.5 \times 10^{-3}$ | 52 | 2430 | 46 |
| DI14B | FM3, FIA, FID | 500 | 45 | 1290 | 28 | $8 \times 10^{-4}$ | 79 | 2230 | 28 |
| D15A | FM3, FIA, FIB, FID | 500 | 51 | 1360 | 27 | $8.6 \times 10^{-4}$ | 88 | 2350 | 27 |

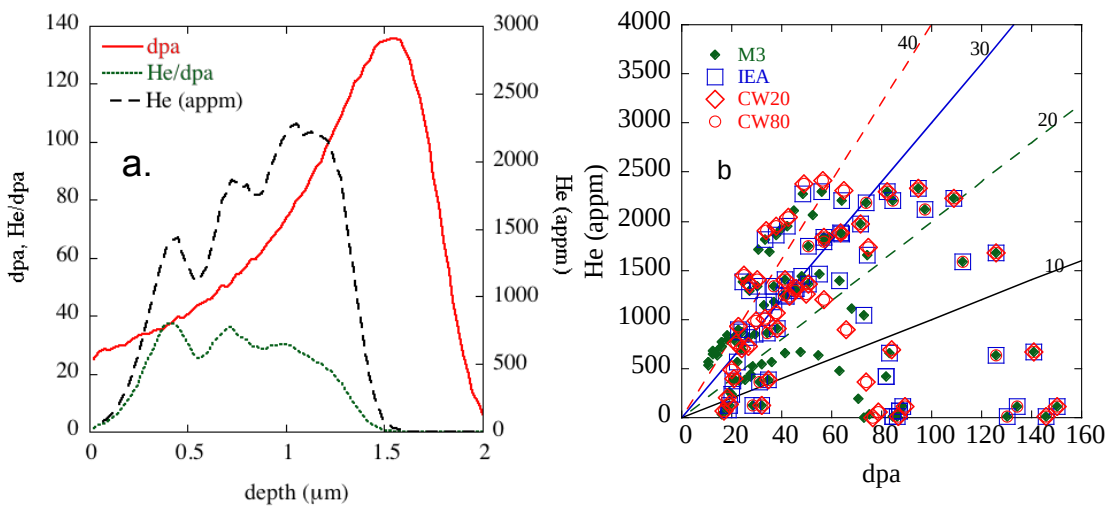


**Figure 1.** a) The dpa, He (appm) and He/dpa profile for DI14B irradiation as an example; and, b) the He/dpa, dpa conditions for all the DI runs for the TMS materials.

For example, areas containing large carbides have a larger number of finer bubbles at the interface, compared to in carbide free regions of the matrix. This local variation in the He bubbles affects the corresponding void $N_v$, $d_v$ and f ($f_v$). Thus we have re-analyzed and added many other areas to previous results. We also found that the pyrometer temperature measurement system may have been miscalibrated during periods when the system upgrades were carried out, leading to possible run-to-run and within run deviations from the nominal 500°C. Hence, for the latest experiment, D15A, the temperature was calibrated every hour using thermocouples welded onto one of the samples, away from the beam area. Using D15A as a reference, all the other runs were analyzed to identify the run-to-run variations. We have also accumulated a significant amount of new data for the F82H IEA steel with 20%

and 80% cold work (CW). These results are tabulated in a large and growing DII database that currently contains 104 dpa-He-dpa rate DII conditions for F82H Mod.3, 64 for as-tempered (AT) F82H IEA, 48 for 20% CW and 64 for 80% CW F82H IEA.

Figure 2 shows the $N_v$, $<d_v>$ and $f_v$ for voids in the as-tempered F82H M3 and IEA groups by the nominal He/dpa ratio based on SRIM estimates rounded to the nearest single digit value in general increments of 10. The filled symbols are for runs in late 2013 (2013B) and early 2014 (2014A). The unfilled symbols are for all the other runs, which are in better agreement with the trends observed in the reference run D15A.

As shown in Figure 2a and 2b, the data group that ran at ≈ nominal temperature (NT) including the reference runs forms a single f vs dpa trend for each He/dpa level. Swelling incubation $dpa_o$ for He/dpa of 40, 30, 20, 10 and <5 are ≈ 40, ≈ 90, ≈ 110 and ≈ 130 (dpa), respectively. Those incubation doses are lower in the other group. While the actual temperatures for the runs were yet to be evaluated, these runs were at ≈ 50°C or more higher temperature (HT) than NT. The HT runs also form consistent trend within themselves showing $dpa_o$ of ≈ 20, ≈ 40, ≈ 60, ≈ 70, and ≈ 80 (dpa) for He/dpa of 40, 30, 20, 10 and <5, respectively. Apparently the effect of He/dpa is more enhanced in NT group.

In the NT group, at the incubation doses especially when f < 1%, $N_v$ increases sharply while $<d_v>$ stays ≈ 5 nm, suggesting that nucleation (transformation from bubbles to voids) is dominant process. For He/dpa = 30 in F82H IEA, the large f ≈ 2% at dpa ≈ $dpa_o$ + 20 is accompanied by a significant growth of voids as $<d_v>$ > 10 nm. In the HT group the $N_v$ and $<d_v>$ trends are different as both increase sharply at the $dpa_o$. These differences can be caused by the difference in the temperature range where void nucleation and/or growth are active. Further investigation of the trends will be covered in a future experiment that will include more systematic and controlled variation of the irradiation temperature.

Figure 3 shows the corresponding a) volume fraction, b) number density, and c) average diameter of "voids" vs. dpa plots for F82H IEA at two CW levels, 20 and 80%. Here we also show the data in the NT and HT groups. Within each group, the trends are consistent and similar to the as-tempered conditions. He/dpa effects on reducing $dpa_o$ is observed in 80% CW.We currently do not have enough data to see the $dpa_o$ in the 20%CW alloy. While the exact HT condition is not determined, in each group the data shows the effect of CW since these 20 vs 80%CW samples were side-by-side irradiated whenever possible. An interesting trend is that the effect of CW on f reverses between HT and NT. At HT larger f is observed in 20%CW, so that including AT, a higher dislocation density (ρ) reduces f, which may be due to a higher number density of smaller bubbles at higher ρ. In the NT condition, higher ρ shows slightly more swelling in all He/dpa levels. ISHI experiments also showed that higher ρ refines bubbles that would otherwise reach critical sizes for void transformation. However, higher ρ enhances the imbalance of vacancies to self-interstitial atoms flowing into cavities. This effect can accelerate void-swelling by reducing the critical size for transformation and increasing void growth rates. These contradicting effects at different temperatures may have resulted in the observed behaviors, but further experimental investigation along with comparison with models are also included in the future study.

**Summary**

This is work in progress and will be discussed in more detail in future reports and publications. The summary of key observations on swelling includes: a) the $f_v$-dpa trend is controlled by the H/dpa; b) better accounting for local microstructure effects and run-to-run variations partly rationalized the observed large data $f_v$ "scatter"; c) $f_v$ is somewhat lower in the reference case and similar runs; d) $f_v$ is lower in M3 than IEA and $f_v$ in IEA decreases with increasing cold work.

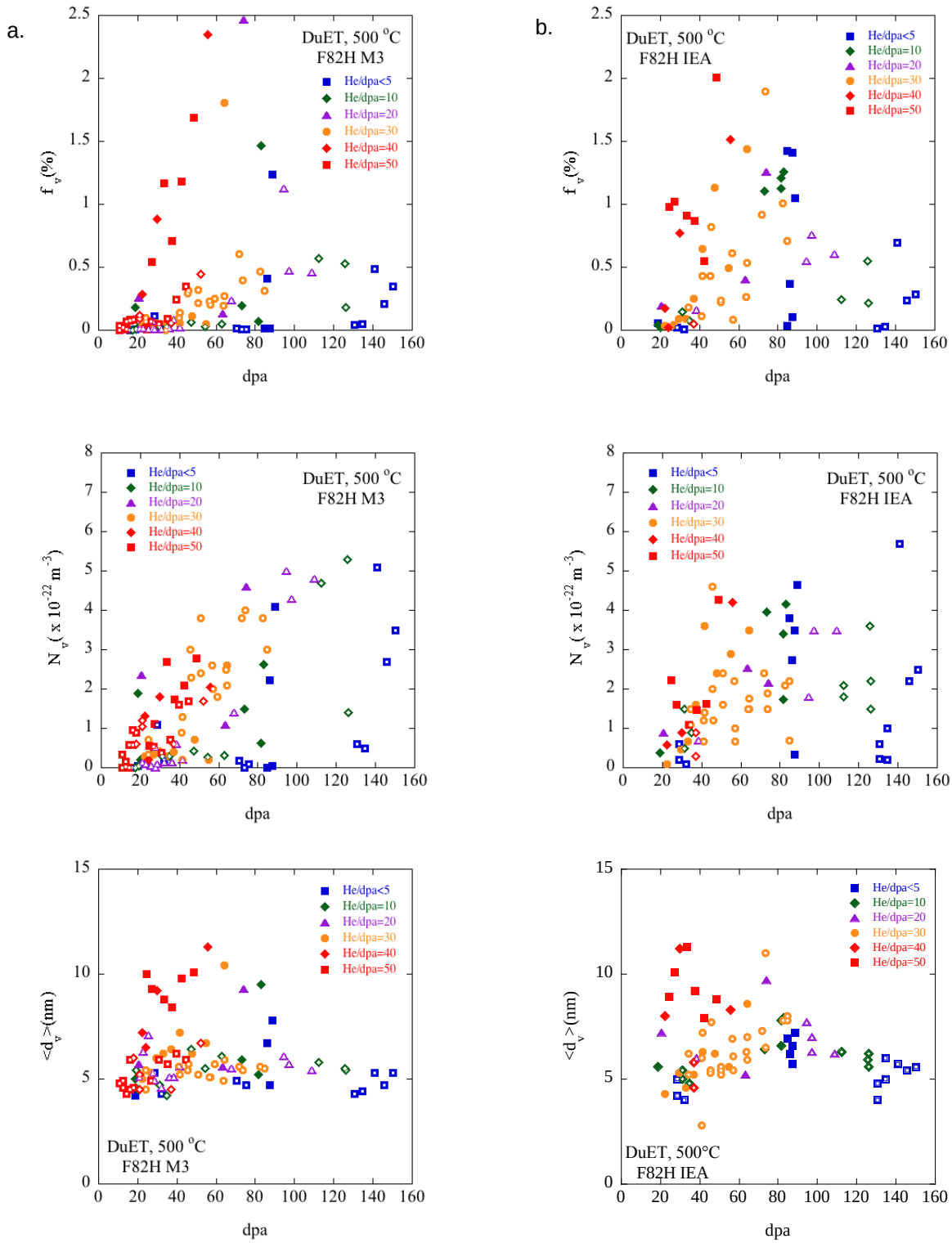


**Figure 2**. The fv, dv and Nv for the as-tempered condition of a) F82H M3; and, b) IEA.

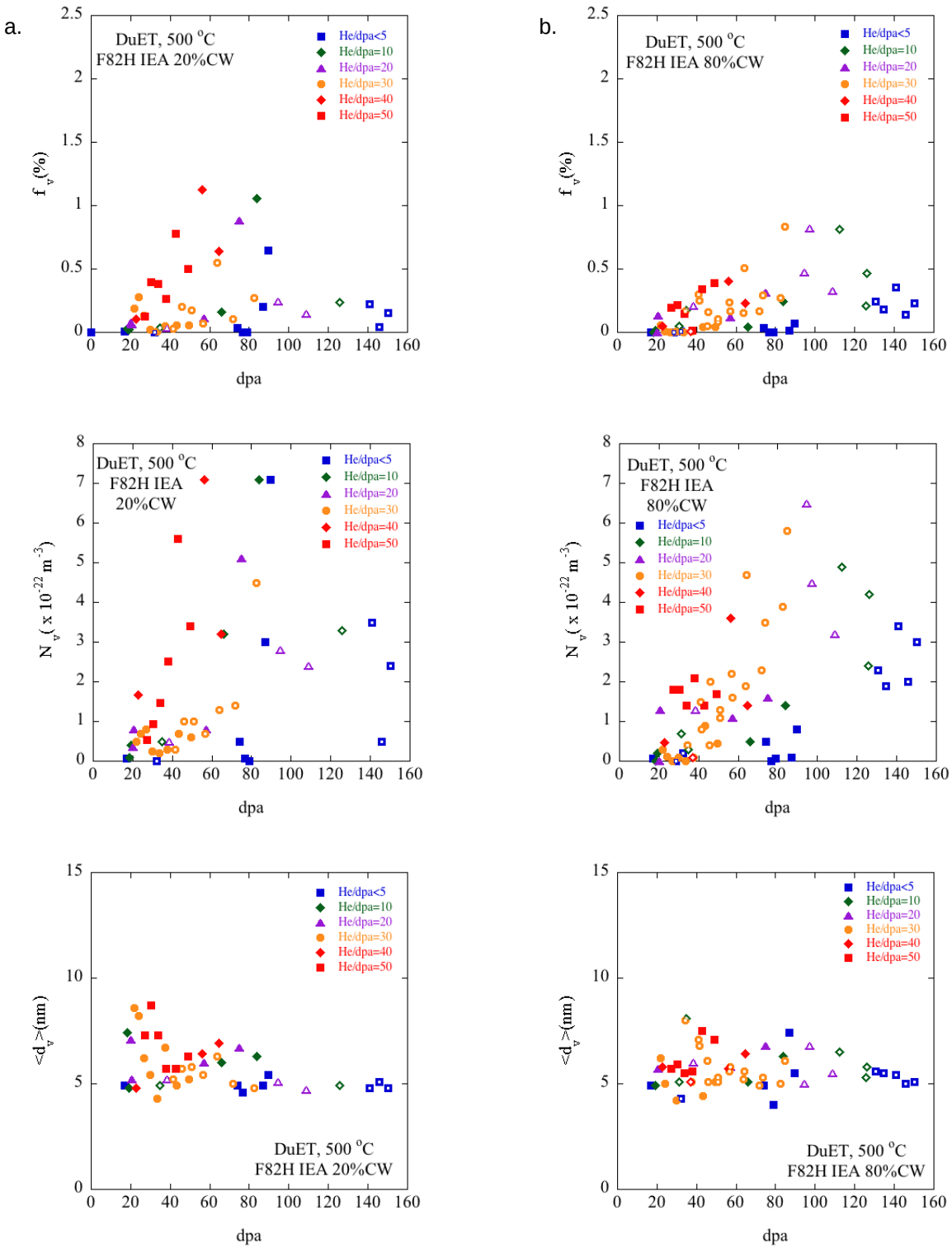


**Figure 3**. The $f_v$, $d_v$ and $N_v$ for the CW conditions of F82H IEA of a) 20%; and, b) 80%.

**Acknowledgements**

The dual ion-beam irradiations were conducted under the support of the “Joint Research Program on Zero-Emission Energy Research, Institute of Advanced Energy, Kyoto University (ZE28A-22, ZE26A-16, 25A-19, 24A-13 and 23B-3). The work performed at UCSB was supported by the U. S. Department of Energy, Office of Fusion Energy Sciences, under contract DE-FG03-94ER54275. We acknowledge the contributions of the NSF sponsored UCSB Microstructure and Microanalysis Facility. We are also grateful for generous support of research materials, F82H mod.3 from Dr. K. Shiba, (JAEA, Japan).

**References (need updates)**

[1] G.R. Odette, T. Yamamoto, Y. Wu, S. Kondo, A. Kimura, *Fusion Materials Semiannual Report 12/31/2014* DOE/ER-313/57 (2015) 8

[2] T. Yamamoto, Y. Wu, G.R. Odette, S. Kondo, A. Kimura, *Fusion Materials Semiannual Report 6/30/2014* DOE/ER-313/56 (2014) 194

[3] T. Yamamoto, Y.Wu, G.R. Odette, K. Yabuuchi, S. Kondo, A. Kimura, J. Nucl. Mater. 449 (2014) 190

[4] T. Yamamoto, Y.Wu, G.R. Odette, S. Kondo, A. Kimura, *Fusion Materials Semiannual Report 6/30/2013* DOE/ER-313/54 (2013) 6.

[5] T. Yamamoto, Y. Wu, G.R. Odette, K. Yabuchi, A. Kimura, *Fusion Materials Semiannual Report 12/31/2010* DOE/ER-313/49 (2011) 1.

[6] ASTM E521-96 (2009), ASTM

[7] R.E. Stoller, M.B. Toloczko, G.S. Was, A.G. Certain, S. Dwaraknath, F.A. Garner, Nuc Instr Mehtods Phys Res B 310 (2013) 75.